Pedothem carbonates reveal anomalous North American atmospheric circulation 70,000–55,000 years ago

Erik J. Oerter[a,1,2], Warren D. Sharp[b], Jessica L. Oster[c], Angela Ebeling[d], John W. Valley[e], Reinhard Kozdon[e,3], Ian J. Orland[e,f], John Hellstrom[g], Jon D. Woodhead[g], Janet M. Hergt[g], Oliver A. Chadwick[h], and Ronald Amundson[a]

[a]Department of Environmental Science, Policy and Management, University of California, Berkeley, CA 94720; [b]Berkeley Geochronology Center, Berkeley, CA 94709; [c]Department of Earth and Environmental Sciences, Vanderbilt University, Nashville, TN 37240; [d]Biology Department, Wisconsin Lutheran College, Milwaukee, WI 53226; [e]Wisconsin Secondary Ion Mass Spectrometer Laboratory, Department of Geoscience, University of Wisconsin, Madison, WI 53706; [f]Department of Earth Sciences, University of Minnesota, Minneapolis, MN 55455; [g]School of Earth Sciences, The University of Melbourne, Melbourne, VIC 3099, Australia; and [h]Department of Geography, University of California, Santa Barbara, CA 93106

Edited by Mark H. Thiemens, University of California, San Diego, La Jolla, CA, and approved December 11, 2015 (received for review August 4, 2015)

Our understanding of climatic conditions, and therefore forcing factors, in North America during the past two glacial cycles is limited in part by the scarcity of long, well-dated, continuous paleoclimate records. Here, we present the first, to our knowledge, continuous, millennial-resolution paleoclimate proxy record derived from millimeter-thick pedogenic carbonate clast coatings (pedothems), which are widely distributed in semiarid to arid regions worldwide. Our new multiisotope pedothem record from the Wind River Basin in Wyoming confirms a previously hypothesized period of increased transport of Gulf of Mexico moisture northward into the continental interior from 70,000 to 55,000 years ago based on oxygen and carbon isotopes determined by ion microprobe and uranium isotopes and U-Th dating by laser ablation inductively coupled plasma mass spectrometry. This pronounced meridional moisture transport, which contrasts with the dominant zonal transport of Pacific moisture into the North American interior by westerly winds before and after 70,000–55,000 years ago, may have resulted from a persistent anticyclone developed above the North American ice sheet during Marine Isotope Stage 4. We conclude that pedothems, when analyzed using microanalytical techniques, can provide high-resolution paleoclimate records that may open new avenues into understanding past terrestrial climates in regions where paleoclimate records are not otherwise available. When pedothem paleoclimate records are combined with existing records they will add complimentary soil-based perspectives on paleoclimate conditions.

paleoclimate | carbon oxygen uranium isotopes | U-series dating | pedogenic carbonate | Marine Isotope Stage 4

During the last two glacial–interglacial cycles, North America experienced some of its most variable and dramatic changes in climate during recent Earth history. These climates were not only temporally dynamic but also, spatially nonuniform (1, 2) in ways that are not yet completely clear. In part, this lack of clarity is because the most informative records—those that are long, continuous, and dated with millennial or better resolution—have been derived primarily from speleothems and/or lake sediments that are absent or rare in large regions of the continent.

In contrast, soil carbonate is nearly ubiquitous in arid and semiarid climates, and pedothems (from Greek: πέδον, *pedon*, "soil"; and θέμα, *théma*, "deposit"), consisting of dense laminated pedogenic carbonate clast coatings, are common in these regions (*SI Appendix*, Fig. S1). After they are formed, pedothems are geochemically closed and retain intact U-Th systematics as evidenced by coherent monotonic age progressions spanning tens of thousands of years (*SI Appendix*, Figs. S2–S4). Stable isotopes of O and C, strongly bound in the carbonate group, also retain their original isotopic compositions and can provide continuous records of paleoclimate conditions for soils that have persisted through millennia of subaerial exposure (3, 4).

Here, we show that micrometer-scale variations in O, C, and U isotopic ratios in carbonate pedothems preserve a continuous, datable record of environmental conditions for the last 120 ka (thousand years) in soils of the Wind River Basin (WR) of northwestern Wyoming. This record was accessed by applying laser ablation U-series dating and ion microprobe C and O stable isotope analyses. Developing this approach and applying it to midcontinent North America allow us to examine a nearly continuous record of the hydroclimates of the most recent glacial cycles in central North America, a region where records of such duration are otherwise unavailable. These data are then compared with other continental records and atmospheric circulation simulations (2, 5–9) to provide deeper insight into the spatial and temporal variabilities in North American paleoclimate.

A midcontinent North American climate record is of particular interest, because previous work (3) has hinted that, during Marine Isotope Stage 4 (MIS 4; 71–57 ka) (10), atmospheric circulation over North America shifted from a state dominated by easterly flow of Pacific Ocean-sourced moisture to one dominated by northerly flow of Gulf of Mexico-sourced moisture into the continental interior. If correct, such a shift in atmospheric circulation should produce an identifiable signal in the O isotope composition of precipitation and

Significance

We show for the first time, to our knowledge, that pedogenic (soil) carbonate mineral accumulations can preserve continuous paleoclimate records that rival the temporal resolution of widely used archives, such as speleothems or lake sediments. Using microanalysis of oxygen, carbon, and uranium isotopes coupled with uranium series dating, we find evidence for a distinct shift in atmospheric circulation in North America's interior from 70,000 to 55,000 years ago, a finding that highlights the influence of large continental ice sheets on atmospheric circulation. Perhaps most significantly, this work shows that pedothems, which are common in arid and semiarid regions around the world, are a rich archive of paleoclimate information for continental landscapes.

Author contributions: E.J.O., W.D.S., O.A.C., and R.A. designed research; E.J.O., W.D.S., A.E., J.W.V., R.K., I.J.O., J.H., J.D.W., J.M.H., O.A.C., and R.A. performed research; E.J.O., W.D.S., and J.L.O. analyzed data; and E.J.O., W.D.S., and R.A. wrote the paper.

The authors declare no conflict of interest.

This article is a PNAS Direct Submission.

[1]To whom correspondence should be addressed. Email: erikjoerter@gmail.com.

[2]Present address: Department of Geology and Geophysics, University of Utah, Salt Lake City, UT 84112.

[3]Present address: Lamont-Doherty Earth Observatory, Columbia University, Palisades, NY 10964.

This article contains supporting information online at www.pnas.org/lookup/suppl/doi:10.1073/pnas.1515478113/-/DCSupplemental.

the productivity of regional flora that are recorded in the O and C isotopic compositions of pedogenic carbonate as we show below.

Carbonate Pedothems

The WR contains a suite of Pleistocene fluvial terraces capped by soils that have persisted through multiple glacial–interglacial climates (3, 4, 11). These soils contain carbonate pedothems consisting of millimeter-thick sequences of conformable laminations attached to the bottoms of alluvial gravel clasts. The O isotopic composition of the carbonate ($\delta^{18}O_c$) should reflect the O isotope composition of precipitation ($\delta^{18}O_p$) (3) mediated by the soil temperature during carbonate precipitation if evaporative enrichment can be excluded as we discuss below. Although $\delta^{18}O_p$ is correlated with atmospheric temperature, storm moisture source and trajectory also play a strong role, especially in midlatitudes (12–14). The C isotope composition of pedogenic carbonate ($\delta^{13}C_c$) is controlled by the proportion of C3- to C4-type vegetation and the soil respiration rate, which are both affected by mean annual temperature and mean annual precipitation (MAP) amount (15, 16). When secondary carbonate forms in soils, U is incorporated at parts per million levels, whereas poorly soluble Th is not; thus, U-series dating techniques may be applied (4, 17). Furthermore, during decay of ^{238}U to its daughter nuclide ^{234}Th, an α-particle (^{4}He) is ejected from the ^{238}U nucleus. The resulting ^{234}Th recoils in the mineral matrix, making it and its daughter ^{234}U vulnerable to mobilization by soil water movement. This process enriches the ^{234}U:^{238}U ratio of soil pore water, with greater enrichment during periods of low soil water flux. As a result, the initial ^{234}U:^{238}U ratio of pedogenic carbonate (^{234}U:$^{238}U_i$), which may be calculated from the measured ^{234}U:^{238}U ratio and the associated U-Th age, is inversely related to the rate of soil water infiltration and reflects changes in paleoprecipitation amount (9, 18). Thus, using these three isotope systems, pedogenic carbonate records past precipitation source, vegetation type and amount, and precipitation amount. In this study, we developed time series of O, C, and ^{234}U:$^{238}U_i$ isotope ratios from transects through laminated pedogenic carbonate clast coatings.

We collected clasts with attached pedothems (*SI Appendix*, Fig. S1) from soil trenches in fluvial terrace 4 of (11) in the WR (43.198°, −108.769°) (Fig. 1). The age of stabilization of the fluvial terrace surface and the onset of soil development is estimated to be 167 ka (±6.4) based on $^{230}Th/U$ dating of the innermost carbonate of pedothem samples collected from various soil depths and analyzed in previous work (4). Two samples from different locations in the 20- to 73-cm-deep soil horizon (samples A-2-07A and A-2-05B) were cut, polished, and inspected to locate regions of dense, translucent primary carbonate. Ages along the transects were constrained by $^{230}Th/U$ dates determined by laser ablation inductively coupled plasma (ICP) -MS on adjacent 93-μm-diameter spots (*Methods*, Fig. 2, and *SI Appendix*, Figs. S2–S4 and Table S1), with age models constructed using the StalAge algorithm (19). Variations in $\delta^{18}O_c$ and $\delta^{13}C_c$ along the transects were measured by ion microprobe using 10-μm-diameter spots (*Methods*, Fig. 2, and *SI Appendix*, Figs. S5–S8 and Tables S2 and S3). These in situ microanalytical techniques provided time series with approximately millennial resolutions over most of their lengths, despite rates of carbonate formation that are typically <100 μm ka^{-1} (Fig. 3*G*).

An essential aspect in determining whether $\delta^{13}C_c$ and $\delta^{18}O_c$ values can be interpreted in terms of climatic influence is the extent to which equilibrium isotopic fractionation during calcite precipitation can be assumed. We performed paired C and O isotope analyses along carbonate laminations on three laminations from sample A-2-07A to examine the isotopic variability within carbonate of similar age (*SI Appendix*, Table S4). These three individual carbonate laminations show variability in $\delta^{13}C_c$ and $\delta^{18}O_c$ values only slightly outside of 2-SD uncertainty limits of individual analysis spots. We interpret these along-lamination transects to confirm that carbonate of similar ages is isotopically homogeneous at the spatial scale of individual secondary ion mass spectrometry (SIMS) analysis spots (~10 μm).

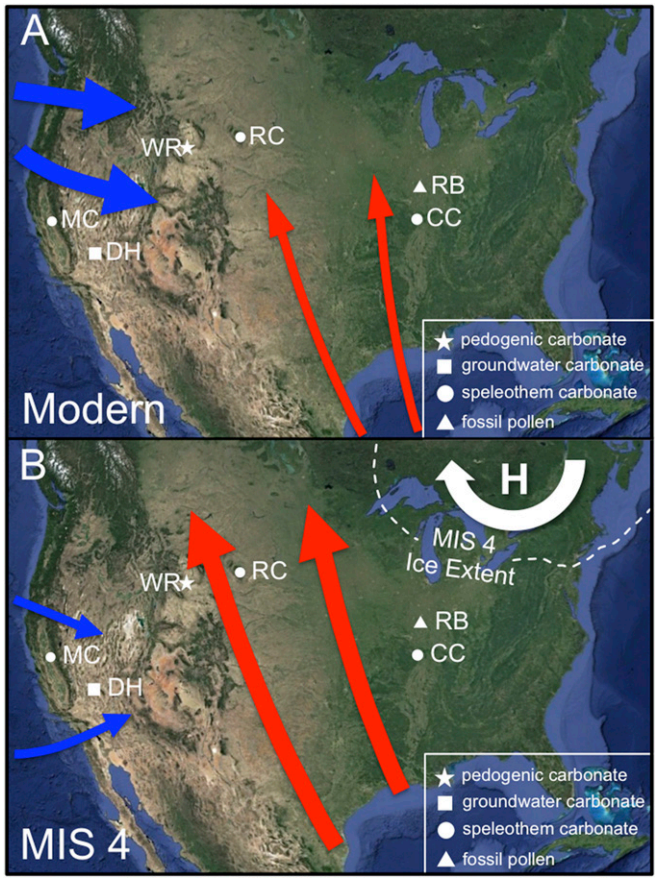

Fig. 1. Maps of (*A*) modern and (*B*) MIS 4 midlatitude North America atmospheric circulation scenarios. Blue arrows denote winter zonal atmospheric circulation; red arrows denote summer meridional circulation. The white arrow denotes persistent MIS 4 anticyclone. Locations are discussed in the text. CC, Crevice Cave, Missouri; DH, Devil's Hole, Nevada; MC, McLean's Cave, California; RB, Raymond Basin, Illinois; RC, Reed's Cave, South Dakota; WR, Wind River Basin, Wyoming.

We measured similar isotope records in three time-transgressive transects on two different samples from different locations in the 20- to 73-cm-deep soil horizon, suggesting that the isotopes reflect conditions inherent to the soil rather than clast-scale processes. Accordingly, we merged results for these three transects into a composite dataset (designated WR A-2). To facilitate comparison with other data, we smoothed temporal trends in WR A-2 with a Gaussian kernel smoother at 0.5-ka bandwidth (Fig. 3 and *SI Appendix*, Figs. S5–S8) (20).

Modern Climate and $\delta^{18}O_c$ and $\delta^{13}C_c$ Values in the WR

The modern mean annual air temperature and MAP at our study site [43.198°, −108.769°; 1,679 m.a.s.l. (meters above sea level)] are 6.3 °C (±0.8 °C) and 231 mm (±70 mm), respectively. Summer [June, July, August, September (JJAS)] mean air temperature and precipitation amounts are 17.2 °C (±3 °C intraseason) and 90 mm (±8 mm intraseason), respectively (21). Nonsummer (months excluding JJAS) precipitation is dominated by zonal storm flow originating in the north Pacific, with average $\delta^{18}O_p$ values of −15.0‰ [Vienna Standard Mean Ocean Water (VSMOW)], and provides 61% of modern MAP. Summer (JJAS) meridional flow with average $\delta^{18}O_p$ values of −10.9‰ (VSMOW) is derived from the Gulf of Mexico and provides 39% of modern MAP (21–23).

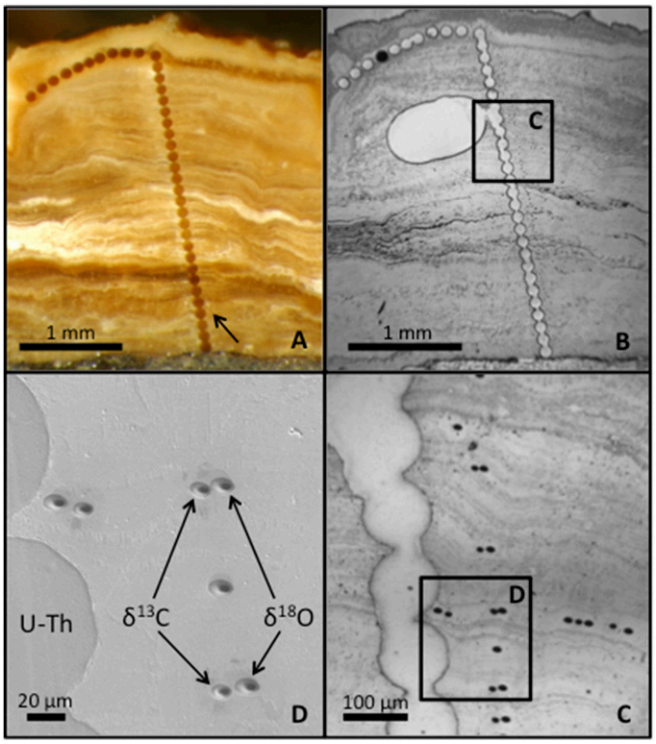

Fig. 2. Reflected light photomicrographs and SEM images of sample A-2-07A Traverse B. (*A*) Laser ablation ICP-MS analysis transects across (time-transgressive; arrow) and along (near-synchronous) pedogenic carbonate laminations. (*B*) ^{230}Th/U calibration sample (light gray; now filled with epoxy) drilled from the white oval with a 300-μm-diameter dental burr and analyzed using the spiked solution ICP-MS technique. (*C*) Magnified area of the box in *B* showing placement of paired SIMS spots for C and O analyses next to laser ablation ICP-MS spots (lighter gray; now filled with epoxy) produced during U-Th analyses for U-series dating and determination of initial U isotope ratios. Multiple SIMS spots along a single carbonate lamination (near center) show the reproducibility of C and O isotopic compositions at near-synchronous positions along the lamination. (*D*) Magnified area of the box in *C* showing detail of the spatial arrangement of C, O, and U-Th analysis spots.

The volume-weighted average annual $\delta^{18}O_p$ value is −13.4‰ (VSMOW).

Calculation of the expected $\delta^{18}O_c$ values of carbonate formed in equilibrium with $\delta^{18}O_p$ (or conversely, estimating past $\delta^{18}O_p$ from observed $\delta^{18}O_c$ values) requires consideration of the seasonality and temperature of soil carbonate formation. Soil carbonate formation occurs during periods of soil dewatering (24) and based on mean temperatures of pedogenic carbonate formation using Δ_{47} ("clumped" isotope) measurements, takes place at a range of temperatures from mean annual air temperature to warmer, depending on the seasonality of precipitation and soil dewatering and soil depth of carbonate formation (25–27). Measurements of pedogenic carbonate formation temperatures using Δ_{47} in southern Wyoming suggest that carbonate forms at temperatures that, in some cases, are 3 °C to 5 °C warmer than summer season air temperatures (i.e., ∼20 °C to 22 °C) (28). Measured $\delta^{18}O_c$ values of Holocene pedogenic carbonates from southern Wyoming at elevations within ±300 m of our study site have an average value of −11.9‰ [Vienna Pee Dee Belemnite (VPDB)] (28). This value is similar to the calculated $\delta^{18}O_c$ of carbonate formed in equilibrium with summer precipitation and summer air temperatures at our study site, which is −11.3‰ (VPDB). These predicted modern and measured Holocene $\delta^{18}O_c$ values are similar to the mid-Holocene $\delta^{18}O_c$ datum obtained from WR A-2 (−10.83‰ at 7.3 ka) (Fig. 3*B* and *SI Appendix*, Table S2). Average $\delta^{13}C_c$ values of pedogenic carbonates in Holocene terraces in the WR are −3.6‰ (±0.6‰; VPDB) (3), similar to the youngest $\delta^{13}C_c$ values in the WR A-2 record (Fig. 3*F* and *SI Appendix*, Table S3). Thus, the C and O isotopic compositions of the youngest laminations in the WR A-2 record are similar to those expected to form under modern conditions.

North American Paleoclimate Revealed by Pedothem Data

The WR multiisotope proxy record reported here begins at 120 ka (Fig. 3*B* and *SI Appendix*, Tables S2 and S3). The sampling frequency from 120 to 70 ka is low because of slow carbonate growth rates, and the $\delta^{18}O_c$ values vary ∼1‰ around a mean of −11.2‰ from 120 to 70 ka. The trend of decreasing $\delta^{13}C_c$ values between 120 and 100 ka (Fig. 3*F*) is interpreted to reflect increases in soil and plant respiration rates. This trend was likely associated with warming temperatures in phase with increasing northern hemisphere summer solar insolation (Fig. 3*A*) after the end of the penultimate glaciation (29). From 100 to 80 ka, $\delta^{13}C_c$ values increase (Fig. 3*F*), suggesting a decrease in soil respiration rates likely caused by colder conditions that inhibit biological activity. A shift in vegetation C3:C4 ratios could explain changes in $\delta^{13}C_c$ values, but there is no evidence of this in the WR region (30).

A sharp increase in $\delta^{18}O_c$ values of ∼2‰ occurs at ∼70 ka, coincident with the onset of MIS 4 (Fig. 3*B*). Several effects could drive such an increase, such as change in the temperature during carbonate formation, increased evaporative enrichment of soil waters, change in the relative proportions of moisture derived from Pacific and Gulf of Mexico sources, or change in the seasonality of soil carbonate formation. It is important to consider the effects of temperature change during MIS 4 when global average temperatures were 2 °C to 5 °C lower than modern temperature (31). Temperature-dependent oxygen isotope fractionation between soil water and carbonate would be expected to yield higher $\delta^{18}O_c$ values at a rate of 0.2‰ °C^{-1} in response to colder temperatures. However, a temperature decrease of 10 °C is required to produce the ∼2‰ increase observed in WR A-2 $\delta^{18}O_c$ values during MIS 4, which is not consistent with MIS 4 summer temperature estimates in Wyoming that are only 2 °C lower than modern temperatures (32). We also note that lower air temperatures should result in lower $\delta^{18}O_p$ values if moisture sources remained the same (12, 13), partially offsetting the effects of lower air and soil temperatures on carbonate–water fractionation.

Higher $\delta^{18}O_c$ values could result from increased evaporation of soil water; however, increased evaporative enrichment during MIS 4 is not consistent with decreased Northern Hemisphere summer insolation (Fig. 3*A*) and global cooling at this time (32, 33). Moreover, model-based simulations of paleoatmospheric circulation indicate that MIS 4 summers were 10–20% more cloudy than modern (32), indicating that the observed increase in $\delta^{18}O_c$ values is not because of ^{18}O enrichment by increased evaporation. Below, we consider change in the relative proportions of moisture sources and change in the seasonality of soil carbonate formation as other explanations for increased $\delta^{18}O_c$ values during MIS 4.

Anomalous Atmospheric Circulation 70,000–55,000 y Ago

Currently, ∼60% of MAP in the WR is derived from the north Pacific and transported by zonal flow during the nonsummer months. The remaining ∼40% of MAP is summer (JJAS) rain and primarily delivered by meridional flow from the Gulf of Mexico (21, 22, 34) (Fig. 1*A*). Holocene carbonate $\delta^{18}O_c$ values in Wyoming at elevations within ±300 m of our study site reflect equilibration at summer soil temperatures, with soil waters having $\delta^{18}O$ values between MAP and summer precipitation (28). Thus, the $\delta^{18}O_c$ values that we observe in the WR A-2 record during MIS 4 most likely also reflect a mixed signal from soil waters derived from both winter and summer precipitation.

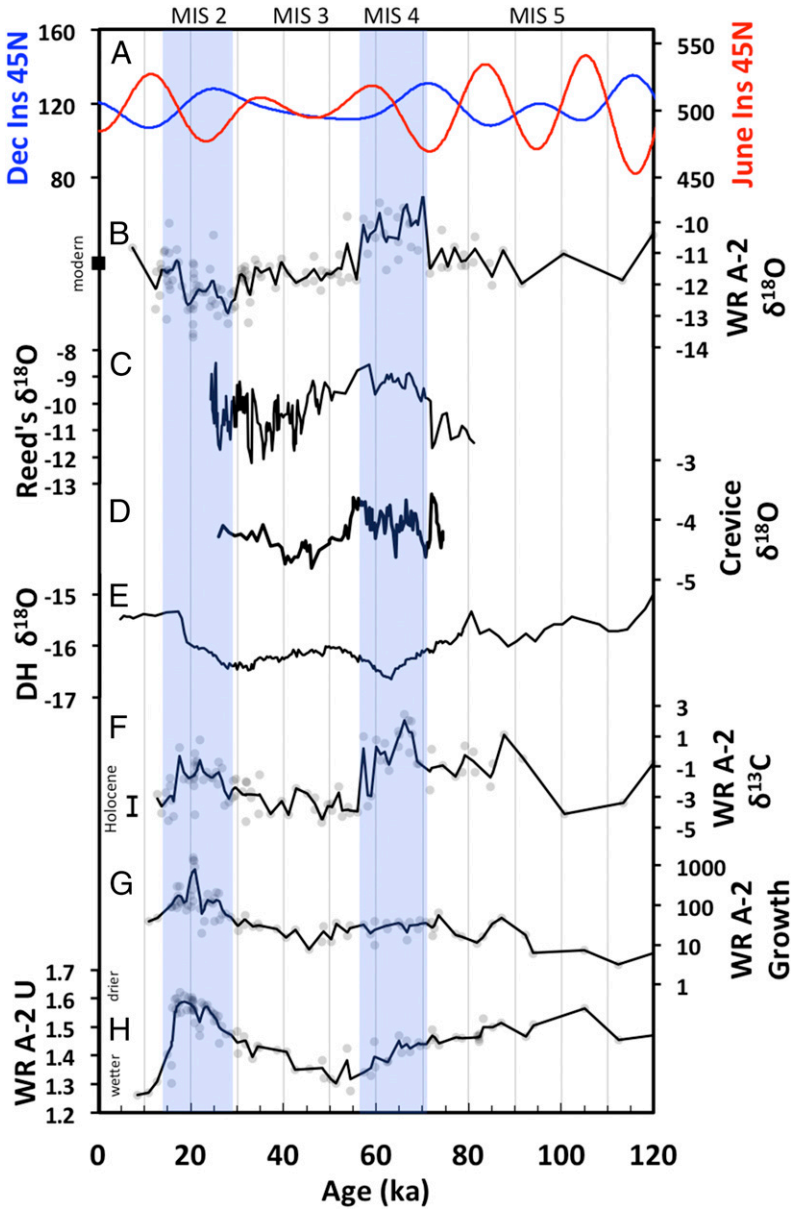

Fig. 3. Comparison of solar insolation and North American paleoclimate records for the last 120 ka; blue-shaded bars denote MISs 2 and 4 (10). WR A-2 records are smoothed trends (thick lines) through data (gray circles), and other records are point to point; WR A-2 $\delta^{18}O_c$ data are ~±0.30‰ (2 SDs), and $\delta^{13}C_c$ data are ~±0.70‰ (2 SDs). (*A*) Solar insolation trends (watts meter^{-2}) at 45° N latitude for June (red) and December (blue) (43). (*B*) WR composite A-2 $\delta^{18}O_c$ record; the black square shows expected modern $\delta^{18}O_c$ calculated from summer average $\delta^{18}O_p$ and summer average air temperatures (21, 23). (*C*) Reed's Cave $\delta^{18}O_c$ record (8). (*D*) Crevice Cave $\delta^{18}O_c$ record (7). (*E*) Devil's Hole (DH) $\delta^{18}O_c$ record (6). (*F*) WR composite A-2 $\delta^{13}C_c$ record; vertical bar shows measured Holocene $\delta^{13}C_c$ values (3). (*G*) WR composite A-2 carbonate growth rate (micrometers ka^{-1}). (*H*) Wind River composite A-2 ^{234}U:$^{238}U_i$ record. All δ values given in per mille (‰) referenced to VPDB standard.

The proportion of Gulf of Mexico- to Pacific-derived precipitation required to produce pedogenic carbonate with $\delta^{18}O_c$ values similar to the WR A-2 record during MIS 4 (–9.87‰ ± 0.87‰, average and SD, respectively, of 10 measurements of $\delta^{18}O_c$ during the period 70–65 ka) (Fig. 2*A* and *SI Appendix*, Table S2) can be estimated by using modern values of seasonal $\delta^{18}O_p$ and considering temperatures estimated to be 2 °C cooler during MIS 4 summers (that is, the summer end member of yearly average decreases of 2 °C to 5 °C) (31, 32). With the O isotope fractionation between water and carbonate corresponding to modern summer soil temperatures less 2 °C, even with 100% Gulf-derived soil moisture, it is difficult to produce $\delta^{18}O_c$ values of –9.87‰. This analysis neglects the effect of cooler temperatures on $\delta^{18}O_p$ values expected during this period, which would reduce $\delta^{18}O_p$ in moisture derived from both Gulf of Mexico and Pacific sources (see above).

Alternatively, we consider two other possibilities to explain the $\delta^{18}O_c$ values observed in the WR record during MIS 4. The first is reduced winter precipitation, leading to an overall decrease in yearly precipitation. However, decreasing ^{234}U:$^{238}U_i$ values in our WR A-2 record during MIS 4 indicate increasing soil water infiltration from more precipitation, less evaporation, or both (Fig. 3*H*), and fossil pollen in the Raymond Basin in Illinois (Fig. 1) indicates that this period was marked by wet summers in the North American midcontinent (35). Another possibility is that wetter summers could have shifted pedogenic carbonate formation into fall. That is, if soils

remained wet through the summer (because of more summer rain and cooler temperatures) and dried during fall at seasonally cooler temperatures, soil carbonate would form in equilibrium with summer $\delta^{18}O_p$ but would do so at cooler fall temperatures, which would increase the resulting $\delta^{18}O_c$ values. We conclude that wetter summers are most consistent with multiple lines of evidence.

During MIS 4, $\delta^{18}O_c$ also increased in speleothems in South Dakota and Missouri (7, 8) (Figs. 1 and 3 *C* and *D*). The similar changes in both soil and cave carbonates indicate a common, regional mechanism for the change in $\delta^{18}O_c$. Thus, the regional increase in $\delta^{18}O_c$ values during MIS 4 is most consistent with a shift in the source or seasonal balance of precipitation in central North America.

WR A-2 $\delta^{13}C_c$ values also peak during MIS 4 (Fig. 3*F*), and given no detectable change in vegetation C3:C4 ratios (30), this increase in $\delta^{13}C_c$ indicates a decline in soil respiration rates, which we attribute to colder average temperatures. Our pedothem evidence together with the other regional paleoclimate records (7, 8, 35) and atmospheric circulation simulations (32) suggest that central North America was characterized by mild, wet summers and cold, dry winters during MIS 4. After MIS 4, the trend toward lower $\delta^{13}C_c$ values after 55 ka indicates increasing plant activity as temperatures warmed while wetter conditions persisted, an interpretation supported by a local minimum in $^{234}U{:}^{238}U_i$ values at ~52 ka (Fig. 3*H*) that is consistent with high soil water infiltration.

The WR A-2 $\delta^{18}O_c$ record for MIS 4 and the Devil's Hole $\delta^{18}O_c$ record from southern Nevada (Fig. 1) undergo shifts during the 70- to 55-ka interval that are coincident but opposite in sign (Fig. 3 *B* and *E*). Devil's Hole reflects aquifer recharge dominated by winter–spring precipitation derived from the Pacific Ocean, and its $\delta^{18}O_c$ values are highly correlated with variations in sea surface temperatures off of California (5, 36). A speleothem from McLean's Cave on the western slope of the Sierra Nevada of California also has lower $\delta^{18}O_c$ and $\delta^{13}C_c$ values at 60 ka, synchronous with the minima in $\delta^{18}O_c$ values in the Devil's Hole record (Fig. 3*E*) (37). Accordingly, Devil's Hole and McLean's Cave both indicate lower temperatures and more ^{18}O-depleted winter precipitation along the western margin of North America during MIS 4 and the MIS 3/4 transition, consistent with cool eastern Pacific surface temperatures. Records of WR $\delta^{18}O_c$ and Devil's Hole $\delta^{18}O_c$ are similar before and after MIS 4 but diverge during MIS 4, indicating distinct atmospheric circulation patterns in the two regions during MIS 4, with Pacific-derived winter precipitation dominant in the west and enhanced Gulf of Mexico-derived summer precipitation over central North America.

MIS 4 was a time of high global ice volume (38), but the North American ice sheet was limited to the northeastern quadrant of the continent (Fig. 1*B*) (39). Atmospheric circulation simulations indicate that a persistent anticyclone developed above the MIS 4 ice sheet, which combined with the eastern location of the ice sheet, created a corridor of northwestward-moving summer winds through central North America, perhaps as far north as Alaska, whereas winters continued to be dominated by largely unchanged westerly winds (32). We interpret the WR A-2 pedothem record as confirmation that the modeled MIS 4 summer atmospheric circulation significantly enhanced transport of Gulf of Mexico moisture to central North America (Fig. 1*B*). During the ensuing period from ~55 to 30 ka (MIS 3), the WR A-2 $\delta^{18}O_c$ and $\delta^{13}C_c$ values show little variability (Fig. 3 *B* and *F*), indicating stable atmospheric circulation regimes and vegetation conditions. Increasing $^{234}U{:}^{238}U_i$ ratios after the start of MIS 3 point to a turn toward drier conditions at the same time that atmospheric circulation reverted to dominance by westerly winds (Fig. 3*H*).

Atmospheric Circulation During and After the Last Glacial Maximum

The onset of the last glaciation (MIS 2) at 29 ka marks the beginning of another major change in North American climate. Compared with that of MIS 4, the MIS 2 Laurentide and Cordilleran ice sheets were much more extensive, spanning North America from west to east, and a large anticyclone developed above it in a midcontinental location (2). Combined with a strong north Pacific high-pressure system and a southward-displaced Aleutian Low, these features steered the jet stream south and away from the WR (2). Sharp increases in WR A-2 $\delta^{13}C_c$ and $^{234}U{:}^{238}U_i$ around the time of the Last Glacial Maximum (LGM) ~21 ka indicate cold and arid conditions in the WR (Fig. 3 *F* and *H*). WR A-2 $\delta^{18}O_c$ values generally decrease during the early part of MIS 2 and reflect the colder temperatures of this glacial period (Fig. 3*B*). Significantly, $\delta^{18}O_c$ values do not show the effect of pronounced northward moisture transport from the Gulf of Mexico as observed during MIS 4. We also note that $\delta^{18}O_c$ values synchronous with the LGM do not seem to reflect evaporative enrichment, even during the driest period of the WR A-2 record (based on $^{234}U{:}^{238}U_i$ values), which further indicates that evaporation was not a significant influence on $\delta^{18}O_c$ throughout the WR A-2 record. Rapid growth of carbonate at this time (Fig. 3*G*), despite indications of low moisture, may be related to high dust input to WR soils during MIS 2 summers as glacial detritus was mobilized from fluvial systems (40).

After the LGM, conditions in the WR quickly changed toward warmer and wetter, with increased $\delta^{18}O_c$ values and decreased $\delta^{13}C_c$ and $^{234}U{:}^{238}U_i$ values (Fig. 3). During the time between the LGM and the end of our WR carbonate record at ~7 ka, the WR A-2 $\delta^{18}O_c$ pattern is generally similar to that of Devil's Hole (Fig. 3 *B* and *E*), although the WR A-2 record shows more detail because of relatively high carbonate growth rates from 25 to 15 ka (Fig. 3*G*). The overall similarity of trends between the WR and Devil's Hole records suggests that both localities were dominated by zonal winter flow of moisture from the Pacific Ocean.

Conclusions

In summary, we show for the first time, to our knowledge, the ability of soil carbonate pedothems to provide long (>100 ka), continuous, well-dated O, C, and U isotope records with millennial or better resolution. The evidence from pedothems of the WR indicates that atmospheric circulation patterns in North America's interior produced a distinctive pattern of moisture transport during MIS 4 (70–55 ka), one of enhanced northward transport of moisture from the Gulf of Mexico and/or a decrease in the amount of Pacific-sourced moisture. The pedothem isotope patterns are consistent with climate simulations, suggesting that an anticyclone developed above the MIS 4 Laurentide ice sheet, affecting regional climate. In contrast, we do not observe a similar O isotope pattern during MIS 2, perhaps because of the much larger extent of the MIS 2 Laurentide and Cordilleran ice sheets and their regional or subcontinental effects on the associated wind directions (2).

The shown ability of pedothems to retain detailed climate information coupled with their analysis by microanalytical techniques offer an exciting new tool for exploring continental responses to global climate changes. Carbonate pedothems are widely distributed in areas that commonly lack more conventional paleoclimate archives and therefore, may provide unique insights into the past climatic conditions of the vast semiarid and arid regions of the planet.

Methods

^{230}Th/U Dating. Laser ablation U-Th analyses were performed at the University of Melbourne using a Nu Plasma MC-ICP-MS coupled to a 193-nm HelEx Laser Ablation System. All U and Th isotopes were measured simultaneously using known ion counter gains, the $^{238}U{:}^{235}U$ ratio to evaluate mass bias, and on-peak baselines. To correct for U-Th fractionation during laser ablation, carbonate samples were milled with 0.3-mm carbide dental burrs along the laser traverses and measured in solution mode at the Berkeley Geochronology Center using a Thermo-Fisher Neptune Plus ICP-MS; $\delta^{13}C_c$ and $\delta^{18}O_c$ analysis spot ages with uncertainties were modeled along the age axis with the StalAge program (19).

$\delta^{18}O_c$ and $\delta^{13}C_c$ Analyses by SIMS. The $\delta^{18}O_c$ and $\delta^{13}C_c$ values were measured by SIMS at the WiscSIMS (Wisconsin Secondary Ion Mass Spectrometer Laboratory) Laboratory, University of Wisconsin, Madison. Samples of the full-thickness

carbonate rinds along with small portions of the attached clasts of 4-mm thickness and 5-mm width were cut from the larger samples and cast into ∼25-mm-diameter epoxy rounds (Buehler Epo-Thin) along with several grains of UWC-3 calcite standard ($\delta^{18}O_c = -17.88‰$ VPDB; $\delta^{13}C_c = -0.91‰$ VPDB) (41). These mounts were polished by hand on rotary disk laps with 9- and then, 3-μm-diameter alumina–water slurry. Additional rotary polishing was done with 3- and 0.25-μm diamond paste in oil followed by a final hand polish with colloidal silica solution (0.05 μm), providing a flat polished surface. The polished samples were then cleaned and sputter-coated with Au to a thickness of ∼60 nm. Samples were inspected with a Hitachi S3400N Scanning Electron Microscope at 1,000× magnification in secondary electron and backscattered electron modes to identify the most suitable SIMS sampling domains according to the criteria of (*i*) the most visible pure carbonate with no inclusions or discernable laminations with no other phases present and (*ii*) no cracks or voids in the sample surface. The large-radius, multicollector CAMECA IMS 1280 at WiscSIMS focuses an ∼1.7-nA $^{133}Cs^+$ primary beam on the sample surface. The primary beam ablates 10-μm-diameter pits to a depth of ∼1 μm by ablating ∼2 ng carbonate. The spot to spot reproducibility values for the data reported here are ≤±0.30‰ 2 SDs for $\delta^{18}O$ and ≤±1.47‰ 2 SDs (but typically ∼±0.70‰) for $\delta^{13}C$. The reproducibility is determined by averaging the results of typically 8 UWC-3 standard analyses that bracket each group of 10–15 sample analyses (42). After SIMS analysis, each analysis pit was imaged by SEM to confirm its location, the absence of cracks or inclusions, and symmetric pit shape.

ACKNOWLEDGMENTS. We thank Ken Ludwig for insights into U-series dating and data analysis, Tim Teague for assistance with sample preparation, Kouki Kitajima for assistance with the WiscSIMS instrument, and Nick Fylstra for assistance with the Berkeley Geochronology Center Neptune ICP-MS. Two anonymous reviewers provided comments and suggestions that improved this paper. Funding was provided by NSF EAR Grants 1329568 (to E.J.O. and R.A.), 0207963 (to W.D.S. and R.A.), and 0207490 (to W.D.S. and R.A.). WiscSIMS is partly supported by NSF Grants EAR03-19230, EAR10-53466, and EAR13-55590. W.D.S. and J.M.H. secured funding from the University of Melbourne Collaborative Research Grant Scheme (International) to conduct the U-series work at the University of Melbourne. I.J.O. was also supported by NSF Grant AGS-1231155.

1. Putnam AE (2015) Palaeoclimate: A glacial zephyr. *Nat Geosci* 8:175–176.
2. Oster JL, Ibarra DE, Winnick MJ, Maher K (2015) Steering of westerly storms over western North America at the Last Glacial Maximum. *Nat Geosci* 23:201–205.
3. Amundson R, Chadwick O, Kendall C, Wang Y, DeNiro M (1996) Isotopic evidence for shifts in atmospheric circulation patterns during the late Quaternary in mid-North America. *Geology* 24(1):23–26.
4. Sharp WD, Ludwig KR, Chadwick OA, Amundson R, Glaser LL (2003) Dating fluvial terraces by ^{230}Th/U on pedogenic carbonate, Wind River Basin, Wyoming. *Quat Res* 59(2):139–150.
5. Winograd IJ, et al. (1992) Continuous 500,000-year climate record from vein calcite in Devils Hole, Nevada. *Science* 258(5080):255–260.
6. Winograd IJ, et al. (2006) Devils Hole, Nevada, $\delta^{18}O$ record extended to the mid-Holocene. *Quat Res* 66(2):202–212.
7. Dorale JA, Edwards RL, Ito E, González LA (1998) Climate and vegetation history of the midcontinent from 75 to 25 ka: A speleothem record from crevice cave, missouri, USA. *Science* 282(5395):1871–1874.
8. Serefiddin F, Schwarcz HP, Ford DC, Baldwin S (2004) Late Pleistocene paleoclimate in the Black Hills of South Dakota from isotope records in speleothems. *Palaeogeogr Palaeoclimatol Palaeoecol* 203(1):1–17.
9. Maher K, et al. (2014) Uranium isotopes in soils as a proxy for past infiltration and precipitation across the western United States. *Am J Sci* 314(4):821–857.
10. Lisiecki LE, Raymo ME (2005) A Pliocene-Pleistocene stack of 57 globally distributed benthic $\delta^{18}O$ records. *Paleoceanography* 20(1):1–17.
11. Evenson EB, Hall RD, Chadwick OA, Sharma P (1997) Cosmogenic Cl-36 and Be-10 ages of Quaternary glacial and fluvial deposits of the Wind River Range, Wyoming. *Geol Soc Am Bull* 109(11):1453–1463.
12. Dansgaard W (1964) Stable isotopes in precipitation. *Tellus B Chem Phys Meteorol* 16(4):436–468.
13. Gat JR (1996) Oxygen and hydrogen isotopes in the hydrologic cycle. *Annu Rev Earth Planet Sci* 24:225–262.
14. Kendall C, Coplen TB (2001) Distribution of oxygen-18 and deuterium in river waters across the United States. *Hydrol Processes* 15(7):1363–1393.
15. Cerling TE (1984) The stable isotopic composition of modern soil carbonate and its relationship to climate. *Earth Planet Sci Lett* 71(2):229–240.
16. Raich JW, Schlesinger WH (1992) The global carbon dioxide flux in soil respiration and its relationship to vegetation and climate. *Tellus B Chem Phys Meterol* 44(2):81–99.
17. Ludwig KR, Paces JB (2002) Uranium-series dating of pedogenic silica and carbonate, Crater Flat, Nevada. *Geochim Cosmochim Acta* 66(3):487–506.
18. Oster JL, Ibarra DE, Harris C, Maher K (2012) Influence of eolian deposition and rainfall amounts on the U-isotopic composition of soil water and soil minerals. *Geochim Cosmochim Acta* 88:146–166.
19. Scholz D, Hoffmann DL (2011) StalAge–an algorithm designed for construction of speleothem age models. *Quat Geochronol* 6(3):369–382.
20. Rehfeld K, Marwan N, Heitzig J, Kurths J (2011) Comparison of correlation analysis techniques for irregularly sampled time series. *Nonlinear Process Geophys* 18(3): 389–404.
21. PRISM Climate Group (2015) *Gridded Climate Data for the Contiguous USA*. Available at prism.oregonstate.edu. Accessed November 16, 2014.
22. Bryson RA, Hare RK (1974) Climates of North America, World Survey of Climatology, eds Bryson RA, Hare RK (Elsevier, New York), Vol 11, pp 1–47.
23. Bowen G, West J, Miller C, Zhao L, Zhang T (2015) *IsoMAP: Isoscapes Modeling, Analysis and Prediction (Version 1.0), The IsoMAP Project.* Available at isomap.rcac.purdue.edu:8080/gridsphere/gridsphere. Accessed November 16, 2014.
24. Breecker DO, Sharp ZD, McFadden LD (2009) Seasonal bias in the formation and stable isotopic composition of pedogenic carbonate in modem soils from central New Mexico, USA. *Geol Soc Am Bull* 121(3-4):630–640.
25. Passey BH, Levin NE, Cerling TE, Brown FH, Eiler JM (2010) High-temperature environments of human evolution in East Africa based on bond ordering in paleosol carbonates. *Proc Natl Acad Sci USA* 107(25):11245–11249.
26. Quade J, Eiler J, Daeron M, Achyuthan H (2013) The clumped isotope geothermometer in soil and paleosol carbonate. *Geochim Cosmochim Acta* 105:92–107.
27. Peters NA, Huntington KW, Hoke GD (2013) Hot or not? Impact of seasonally variable soil carbonate formation on paleotemperature and O-isotope records from clumped isotope thermometry. *Earth Planet Sci Lett* 361:208–218.
28. Hough BG, Fan M, Passey BH (2014) Calibration of the clumped isotope geothermometer in soil carbonate in Wyoming and Nebraska, USA: Implications for paleoelevation and paleoclimate reconstruction. *Earth Planet Sci Lett* 391:110–120.
29. Broecker WS, Henderson GM (1998) The sequence of events surrounding Termination II and their implications for the cause of glacial-interglacial CO_2 changes. *Paleoceanography* 13(4):352–364.
30. Baker RG (1983) Holocene vegetation history of the Western United States. *The Holocene*, Late Quaternary Environments of the United States, ed Wright HEJ (Univ of Minnesota Press, Minneapolis), Vol 2, pp 109–127.
31. Sachs JP, Lehman SJ (1999) Subtropical North Atlantic temperatures 60,000 to 30,000 years ago. *Science* 286(5440):756–759.
32. Löfverström M, Caballero R, Nilsson J, Kleman J (2014) Evolution of the large-scale atmospheric circulation in response to changing ice sheets over the last glacial cycle. *Clim Past Discuss* 10(4):1453–1471.
33. Petit JR, et al. (1999) Climate and atmospheric history of the past 420,000 years from the Vostok ice core, Antarctica. *Nature* 399(6735):429–436.
34. Liu ZF, Bowen GJ, Welker JM (2010) Atmospheric circulation is reflected in precipitation isotope gradients over the conterminous United States. *J Geophys Res Atmos* 115:D22120.
35. Curry BB, Baker RG (2000) Palaeohydrology, vegetation, and climate since the late Illinois Episode (∼130 ka) in south-central Illinois. *Palaeogeogr Palaeoclimatol Palaeoecol* 155(1):59–81.
36. Coplen TB (2007) Calibration of the calcite–water oxygen-isotope geothermometer at Devils Hole, Nevada, a natural laboratory. *Geochim Cosmochim Acta* 71(16):3948–3957.
37. Oster JL, et al. (2014) Millennial-scale variations in western Sierra Nevada precipitation during the last glacial cycle MIS 4/3 transition. *Quat Res* 82(1):236–248.
38. Andersen KK, et al.; North Greenland Ice Core Project members (2004) High-resolution record of Northern Hemisphere climate extending into the last interglacial period. *Nature* 431(7005):147–151.
39. Kleman J, et al. (2010) North American Ice Sheet build-up during the last glacial cycle, 115–21kyr. *Quat Sci Rev* 29(17):2036–2051.
40. Pierce KL, et al. (2011) A loess–paleosol record of climate and glacial history over the past two glacial–interglacial cycles (∼150ka), southern Jackson Hole, Wyoming. *Quat Res* 76(1):119–141.
41. Kozdon R, Ushikubo T, Kita N, Spicuzza M, Valley JW (2009) Intratest oxygen isotope variability in the planktonic foraminifer N. pachyderma: Real vs. apparent vital effects by ion microprobe. *Chem Geol* 258:327–337.
42. Kita NT, Ushikubo T, Fu B, Valley JW (2009) High precision SIMS oxygen isotope analysis and the effect of sample topography. *Chem Geol* 264(1-4):43–57.
43. Laskar J, et al. (2004) A long- term numerical solution for the insolation quantities of the Earth. *Astron Astrophys* 428(1):261–285.